Mechanism of Selective Oxidation of Propene to Acrolein on Bismuth Molybdates from Quantum Mechanical Calculations

Sanja Pudar, Jonas Oxgaard, Kimberly Chenoweth, Adri C. T. van Duin, and William A. Goddard, III*

Materials and Process Simulation Center (139-74), California Institute of Technology, Pasadena, California 91125

Received: June 8, 2007; In Final Form: July 29, 2007

In order to provide a basis for understanding the fundamental chemical mechanisms underlying the selective oxidation of propene to acrolein by bismuth molybdates, we report quantum mechanical studies (at the DFT/B3LYP/LACVP** level) of various reaction steps on bismuth oxide (Bi_4O_6/Bi_4O_7) and molybdenum oxide (Mo_3O_9) cluster models. For CH activation, we find a low-energy pathway on a Bi^V site with a calculated barrier of $\Delta H^{\ddagger} = 11.0$ kcal/mol ($\Delta G^{\ddagger} = 30.4$ kcal/mol), which is ~3 kcal/mol lower than the experimentally measured barrier on a pure Bi_2O_3 condensed phase. We find this process to be not feasible on Bi^{III} (it is highly endothermic, $\Delta E = 50.9$ kcal/mol, $\Delta G = 41.6$ kcal/mol) or on pure molybdenum oxide (prohibitively high barriers, $\Delta E^{\ddagger} = 32.5$ kcal/mol, $\Delta G^{\ddagger} = 48.1$ kcal/mol), suggesting that the CH activation event occurs on (rare) Bi^V sites on the Bi_2O_3 surface. The expected low concentration of Bi^V could explain the 3 kcal/mol discrepancy between our calculated barrier and experiment. We present in detail the allyl oxidation mechanism over Mo_3O_9, which includes the adsorption of allyl to form the π-allyl and σ-allyl species, the second hydrogen abstraction to form acrolein, and acrolein desorption. The formation of σ-allyl intermediate is reversible, with forward $\Delta E^{\ddagger}$ ($\Delta G^{\ddagger}$) barriers of 2.7 (9.0 with respect to the π-allyl intermediate) kcal/mol and reverse barriers of 21.6 (23.7) kcal/mol. The second hydrogen abstraction is the rate-determining step for allyl conversion, with a calculated $\Delta E^{\ddagger} = 35.6$ kcal/mol ($\Delta G^{\ddagger} = 37.5$ kcal/mol). Finally, studies of acrolein desorption in presence of gaseous O_2 suggest that the reoxidation significantly weakens the coordination of acrolein to the reduced Mo^{IV} site, helping drive desorption of acrolein from the surface.

1. Introduction

Catalytic oxidation of small olefins to unsaturated aldehydes and catalytic ammoxidation of small olefins to nitriles is of major commercial importance, representing 25% of the chemicals used in the manufacture of industrial and consumer products. In particular, about eight billion pounds of acrolein is produced annually,[1] primarily through catalytic oxidation of propene (eq 1)

$$CH_3CH{=}CH_2 + O_2 \xrightarrow[\text{cat.}]{300-450\ ^\circ C} CH_2{=}CHCHO\ (\text{acrolein}) + H_2O \quad (1)$$

In the early stages of this industry, acrolein was produced on simple bismuth and molybdenum oxide catalysts, but incorporation of other metals has significantly increased yield and selectivity. Even so, this process is still not optimal and even small improvements in the efficiency of the catalyst can have a major effect on environmental impact and energy requirements.

Due to the commercial importance of this process, many fundamental studies have been directed toward the understanding of the selective oxidation on Bi/Mo catalysts, yet there is still considerable uncertainty about the detailed chemical mechanisms involved. To gain more insight into this process and to lay a foundation for improving the catalysts, we have used quantum mechanical (QM) methods (at the DFT/B3LYP/LACVP** level) in conjunction with cluster models of the component oxides (Bi_2O_3 and MoO_3) to investigate the various steps involved in oxidizing propene to acrolein.

In our study we investigated the mechanism outlined in Scheme 1,[2,3] consisting of the following steps:

1. Propene coordination to the catalyst.
2. Allylic hydrogen abstraction by oxygen associated with bismuth (TS_{A-B} in Scheme 1) to form a π-allyl intermediate (B).
3. C−O bond formation on a molybdenum site to form a σ-allyl intermediate (C).
4. A second hydrogen abstraction on a molybdenum site (TS_{C-D}) to form acrolein and a reduced Mo (D).
5. Reoxidation of the active site by lattice oxygen migration and filling of the vacancy by gaseous dioxygen.

1.1. Overview of Experimental Work. Experiments by Burrington and Grasselli[4] showed that at 320 °C, the rates of propene oxidation on Bi/Mo catalysts decrease in following order:

$$(M_a^{2+}M_b^{3+}Bi_xMo_yO_x) > Bi_2O_3{\cdot}2MoO_3 \approx Bi_2O_3{\cdot}3MoO_3 > Bi_2O_3{\cdot}MoO_3 > MoO_3 \approx Bi_2O_3$$

Pure α-Bi_2O_3 is found not to oxidize propene to acrolein but gives traces of 1,5-hexadiene, CO_2, and benzene. The 1,5-hexadiene is the expected product of allyl radical dimerization, suggesting that propene is activated on α-Bi_2O_3 but no further reaction occurs.[4−7] In addition, no oxidation occurs when

* Corresponding author. E-mail: wag@wag.caltech.edu.

10.1021/jp074452a CCC: $37.00
Published on Web 10/11/2007

SCHEME 1: Proposed Mechanism for Propene Oxidation over Bismuth Molybdates[a]

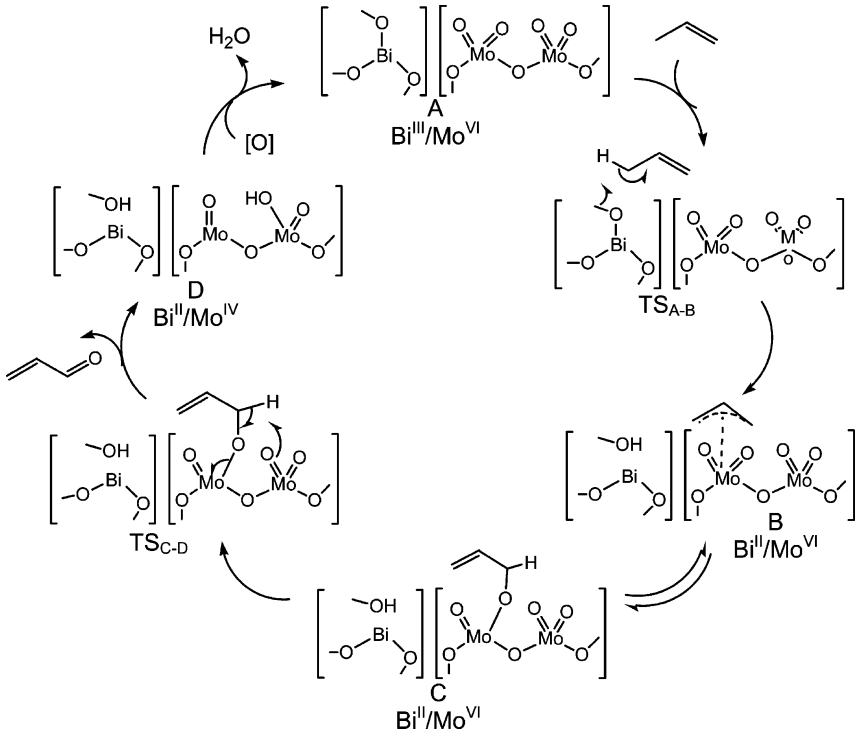

[a] Refs 2 and 3.

propene is exposed to pure MoO_3, most likely because MoO_3 is not capable of carrying out the first CH activation event. Burrington and Grasselli studied the reaction of MoO_3 with azopropene (which readily generates free allyl radicals) and reported a normalized acrolein yield of 51.5% (as well as 14.9% acetaldehyde, 14.7% CO_2, 11.4% benzene, and 7.6% propene).[4] Somewhat contrary, Martir and Lunsford reported that if Bi_2O_3 is placed upstream of MoO_3 in a flow reactor, only a small amount of acrolein is produced, and concluded that conversion of allyl radicals to acrolein is not very efficient over pure MoO_3.[8] However, the difference in acrolein yields may be caused by the difference in experimental conditions and setup. In addition, the sequential placement of Bi_2O_3 and MoO_3 reduced the amount of allyl radicals by a factor of 20, suggesting that MoO_3 acts as a radical scavenger.

Experimental studies also suggest that the rate-determining step is a α-methyl hydrogen abstraction to form allylic radical intermediates. This was established from both the kinetic isotope effect (KIE) ($k_H/k_D = 1.82$) and the isotopic distributions of oxygen insertion products from either allyl- or vinyl-D-labeled propenes.[9−12] Martir and Lunsford reported an activation energy of 14 kcal/mol for allyl radical formation over pure Bi_2O_3,[8] over the temperature range of 523−723 K. However, White and Hightower reported an activation energy of 22 kcal/mol for the catalytic reaction of propene and oxygen to form 1,5-hexadiene over Bi_2O_3,[13] whereas Swift et al. reported the value of 27.5 kcal/mol for cyclic reduction of Bi_2O_3 by propene.[6] It is not clear why these reported values are so distinctly different, although it should be noted that the studies employ a wide range of experimental conditions. The experimental activation energy for α-methyl hydrogen abstraction on mixed bismuth molybdates is seemingly less controversial and has been reported as 19−21 kcal/mol.[2]

Subsequent steps in the conversion of allyl intermediate to acrolein have been studied over molybdates using molecular probes, such as allyl alcohol, allyl amine, and selected D- and ^{18}O-labeled derivatives.[4,14−17] According to the observed isotopic distributions of acrolein-3,3-d_2 and 1-d_1 in oxidation of either allyl alcohol-1,1-d_2 and -3,3-d_2, or propene-1,1-d_2 and -3,3,3-d_3, the initial rate-determining step results in the formation of a π-allyl intermediate, where allyl is π-bonded to a coordinately unsaturated Mo. This π-allyl species is rapidly and reversibly converted to a σ-allyl intermediate (the acrolein precursor) through the formation of a C−O bond, which is followed by the second hydrogen abstraction to give acrolein. The second hydrogen abstraction is the slow step in the conversion of the σ-allyl species to acrolein.

While it is clear that the first C−H activation event occurs on the bismuth and the subsequent oxidation occurs on the molybdenum, the difference between Martir and Lunsford's sequential Bi/Mo setup and the commercial mixed Bi/Mo catalysts (such as $Bi_2O_3 \times 3MoO_3$ and $Bi_2O_3 \times 2MoO_3$) suggests that the functions of Bi_2O_3 and MoO_3 are not merely additive.[4] The selectivity to acrolein of simple bismuth molybdates is about 90%, with only trace amounts of CO, CO_2, and acetaldehyde being formed, which should be compared to the 51.5% acrolein yield of the pure MoO_3 reacting with allyl radicals.[4] The nature and cause of this nonadditive effect has not yet been explained.

1.2. Earlier Theoretical Work. Jang and Goddard previously studied the thermodynamics of propene activation by Bi^{III} using a Bi_4O_6 cluster model.[18,19] They found that the energy cost for the first hydrogen abstraction by oxygen is endothermic by 50.9 kcal/mol ($\Delta G_{673K} = 41.6$ kcal/mol), possibly because it leads to Bi−O bond cleavage and produces a very unfavorable reduced Bi^{II} state. These results appear contrary to the widely accepted view that the Bi^{III} site is responsible for activation of propene.

Jang and Goddard also considered propene activation on a Bi^V site using a Bi_4O_7 cluster model, which has two different types of oxygens, bridging oxygens and terminal oxo oxygen. They found that the Bi^V oxidized site leads to favorable C−H activation (due to favorable reduction of Bi^V to Bi^{IV}) with a reaction energy $\Delta E = 6.4$ kcal/mol ($\Delta G_{673K} = 2.5$ kcal/mol).

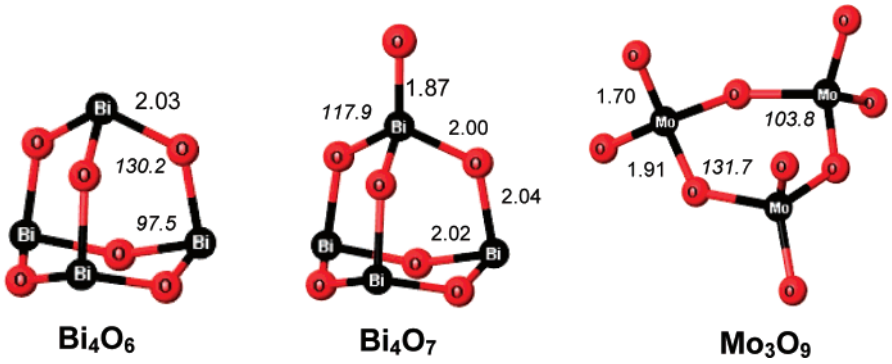

Figure 1. Cluster models used to represent the Bi^{III} site in Bi_4O_6, the Bi^{V} site in Bi_4O_7, and the Mo^{VI} site in Mo_3O_9. Selected bond lengths and angles are shown in angstroms and degrees, respectively.

In addition, they found that activating another propene at the Bi^{IV} site is exothermic with a $\Delta E = -14.4$ kcal/mol ($\Delta G_{673K} = -35.9$ kcal/mol). Indeed it is known that Bi_2O_3 has the ability to chemisorb O_2 dissociatively,[20] suggesting that in an oxidizing environment O_2 reacts with surface Bi^{III} to form very small amounts of Bi^{V} species. However, Jang and Goddard calculated that the energy cost for formation of this Bi^{V} species by dissociative chemisorption of O_2 molecule was high, $\Delta E = 27.5$ kcal/mol ($\Delta G_{673K} = 36.9$ kcal/mol). Since this energy includes half the dissociation energy of oxygen into atomic oxygens, Jang and Goddard suggested that this energy cost might be lowered significantly if the oxygen molecule dissociatively chemisorbs on some other site, such as Fe(II), and migrates to the bismuth site. Indeed, multicomponent catalysts that include Fe components show drastic improvement over simple bismuth molybdates, which was attributed mainly to improved activation of O_2 to atomic lattice oxygen by the Fe(II)/Fe(III) redox couple.[21]

Jang and Goddard also studied the thermodynamics of the allyl adsorption on Bi^{III} and Mo^{VI} sites. They found that adsorption of allyl on Bi^{III} has a high energy cost ($\Delta G_{673K} = 31.0$ kcal/mol), due formation of the unfavorable Bi^{II} state upon cleavage of the Bi−O bond. Thus the only plausible pathway over Bi_2O_3 is the dimerization of allyl radicals. In contrast, chemisorption of allyl on the molybdenum terminal oxo sites is quite favorable ($\Delta G_{673K} = 5.7$ kcal/mol). In addition, Jang and Goddard concluded that the second hydrogen abstraction step is most favorable when it occurs on a terminal oxo group of an adjacent molybdenum site.[18,22]

While Jang and Goddard's thermodynamic studies yielded significant insight into the chemistry of this process, they did not calculate the barriers for the various reaction steps, leaving uncertainties in their proposed mechanism. We now report the complete quantum mechanics based mechanism for propene oxidation on Bi_2O_3 and MoO_3, including barriers. This report concentrates on cluster models of pure Bi_2O_3 and MoO_3, without mixing of metals, in order to establish the fundamental mechanistic steps.

2. Technical Details

2.1. Theoretical Methodology. All calculations were performed using the B3LYP flavor of density functional theory (DFT), which combines exact HF exchange with the Becke generalized gradient exchange function[23] and the Lee, Yang, and Parr correlation functional (LYP).[24] Molybdenum and bismuth were described using the LACVP relativistic effective core potentials and basis sets of Hay and Wadt[25] which treat explicitly 14 valence electrons on molybdenum and 5 valence electrons on bismuth. The O, C, and H atoms were described using the Pople 6-31G** basis set, including core and valence electrons. Closed shell species were studied using RDFT, whereas UDFT was used for open shell species.

Geometries were fully optimized for each structure reported. The minima and saddle points were confirmed by diagonalizing the Hessian matrix and computing the vibrational frequencies. Each minimum had no imaginary frequencies, and each transition state was confirmed to be a first-order saddle point (one imaginary frequency). The vibrational frequencies were used to calculate zero-point energy (ZPE) and enthalpies at 0 K for each structure, as well as to calculate the enthalpy and entropy corrections to the QM energies at the experimental reaction temperature, 593 K. No frequency scaling term was used in calculating ZPE or thermodynamic properties. All calculations were carried out with the Jaguar 6.5 program.[26]

2.2. Cluster Models. In this work we explore C−H propene activation on pure bismuth and molybdenum oxide model cyclic clusters, Bi_4O_6 and Mo_3O_9, respectively, as shown in Figure 1. The allyl conversion to acrolein was studied on a pure molybdenum oxide cyclic cluster model, Mo_3O_9. The cyclic cluster models were used to avoid having to terminate the clusters with OH species.

The crystal structure of α-Bi_2O_3 shows that each bismuth is connected to three nearest-neighbor oxygens, with each oxygen connected to two bismuth atoms.[27] Bismuth oxide vaporization experiments show that the gas phase consists of large amounts of closed shell $(Bi_2O_3)_n$ clusters, including a neutral and stable Bi_4O_6 species.[28−30] It has been proposed that Bi_4O_6 has a compact cage structure with tricoordinated bismuth and bicoordinated oxygens.[28,30] Experiments on scattered bismuth oxide clusters $(Bi_2O_3)_nBiO^+$ ($1 \le n \le 4$) with ethene and propene show strong activity, suggesting that the isolated cluster has chemistry similar to that of bulk Bi_2O_3.[31] In addition, evidence of catalytic activity of $Bi_4O_6^+$ toward alkenes via activation of molecular oxygen has been reported.[32] Thus, the cyclic Bi_4O_6 cluster appears to mimic the chemistry and to retain the stoichiometry, neutrality, and coordination of bulk Bi_2O_3. Consequently we chose this cluster to represent the active site for propene activation (Figure 1). This cluster model has been used previously in theoretical studies of (amm)-oxidation of propene[18,19] and of bismuth oxide reactivity toward ethane and molecular oxygen.[33] For investigations of Bi^{V} we modified the Bi_4O_6 to include an extra terminal oxygen on one Bi, resulting in a $Bi^{III}_3Bi^{V}O_7$ cluster (abbreviated Bi_4O_7). Since the number of Bi^{V} sites on the real surface should be low, this is a more realistic model than a "pure" Bi^{V}cluster, such as $Bi^{V}_4O_{10}$.

The crystal structure of MoO_3 has two oxygen neighbors at an average distance of 1.68 Å (Mo═O oxo bonds), two oxygens at a distance of 2.02 Å (Mo−O−Mo bonds), and two oxygens at 2.3A (donor−acceptor bonds) as shown in Figure 2.[34] Thus,

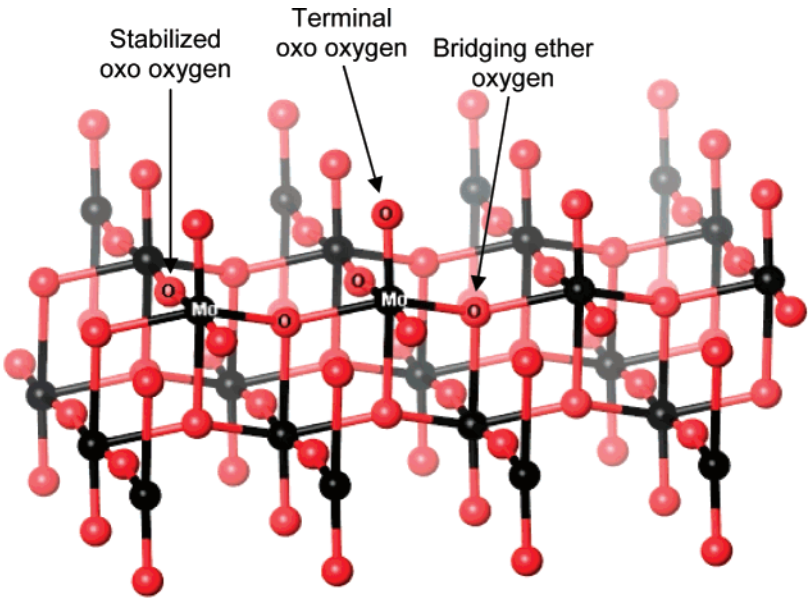

Figure 2. Types of oxygen atoms on the α-MoO_3(010) surface. The terminal and stabilized oxo oxygen distances to the bonded Mo are both 1.68 Å while the Mo− O−Mo ether-like single bonds are 2.02 Å.

this Mo is sometimes referred to as a distorted octahedron and sometimes as a distorted tetrahedron. Thus, there are three kinds of structurally different lattice oxygens in MoO_3: (1) *terminal* oxo oxygen, making an oxo bond to one molybdenum with a Mo−O distance of 1.68 Å, (2) *stabilized oxo* oxygen, making an oxo bond to one molybdenum with a Mo−O distance of 1.68 Å and weakly coupled in a donor−acceptor bond to another surface molybdenum at a distance of 2.30 Å, and (3) *ether bridging* oxygen atoms singly bonded to two surface molybdenum atoms at a distance of 2.02 Å, and weakly coupled in a donor−acceptor bond with a Mo of the underlying sublayer, at a distance of 2.31 Å. A similar bonding configuration is found in α-$Bi_2Mo_3O_{12}$, one of the most active mixed Mo/Bi catalysts.[35]

Evaporation of MoO_3 samples from a Knudsen effusion source shows an abundance Mo_3O_9 clusters in the vapor, which is proposed to have a six-membered ring structure as in Figure 1.[36,37] There have been several experiments on the reaction of these gas-phase molybdenum oxide clusters with small alcohols, alkanes, alkenes, and ammonia as a model study for mechanisms of heterogeneous catalysis.[37,38] These observations show that Mo_3O_9 type clusters are reactive toward oxidation of CO, C−C activation of cyclopropane and propene, and dehydrogenation of NH_3. Thus, we chose the Mo_3O_9 cluster to represent the active molybdenum site for oxidation (Figure 1). It has reactivity, stoichiometry, and coordination similar to that found in both pure MoO_3 and α-$Bi_2Mo_3O_{12}$ catalysts (see Figure 2). In this cluster model, each molybdenum is coordinated to two terminal oxo oxygens and two bridging or ether oxygens, corresponding to oxo and ether bridging oxygens in the MoO_3 crystal. This cluster model was also used by Goddard and Jang in a mechanistic study of (amm)-oxidation of propene,[18,19] and by Fu et al. to study methane and propane activation.[39,40]

3. Results

Earlier work on this topic by Jang and Goddard explored the thermodynamics of various pathways, which we extend here to also include the relevant barriers. Propene activation is studied on bismuth and molybdenum oxides, and allyl intermediate conversion to acrolein on molybdenum oxide.

3.1. Propene Activation. *3.1.1. Bi_4O_7 Cluster.* As concluded from our previous work, we find that Bi^{III} is not able to activate the allylic C−H bond of propene. Thus, we investigated the reactivity of the Bi^V toward propene activation. The potential energy surface (singlet spin state) for this process is shown in Figure 3. Here species **2** is propene weakly coordinating to a Bi^V oxo oxygen, with a $\Delta E = -1.9$ kcal/mol ($\Delta G_{593K} = 19.9$ kcal/mol). This low energy of coordination (indeed, endothermic on the free energy surface) agrees with the observation by Matsuura that propene adsorption on Bi_2O_3 is weak compared to adsorption on MoO_3 and $BiMoO_6$.[41] As shown in Figure 3, **2** features a methyl hydrogen coordinating to an oxo oxygen, with a H−O distance of 2.29 Å. Another isomer is found at $\Delta E = -2.0$ kcal/mol ($\Delta G = 22.2$ kcal/mol), where the hydrogen on the middle carbon coordinates to the oxo at distance of 2.23 Å.

The $\Delta E^{\ddagger}$ of activation for the first hydrogen abstraction is 14.7 kcal/mol ($\Delta G^{\ddagger}_{593K} = 30.4$ kcal/mol), with a transition state imaginary frequency of $\nu = 665$i cm^{-1} corresponding to the hydrogen abstraction by an oxo oxygen. In the transition state structure **TS1** (Figure 4) the Bi═O bond has increased from 1.87 to 2.07 Å, the methyl C−H bond has increased from 1.10 to 1.40 Å, and the O−H distance is decreased from 2.29 to 1.08 Å with respect to **2**. These bond distances indicate that the allyl radical is almost fully formed. However, the two C−C bonds are 1.45 and 1.35 Å, indicating that the allyl radical with its equivalent CC bond distances has not yet formed. Furthermore, the UDFT $\langle S^2 \rangle$ value is 0.000, consistent with the closed shell character of this species, which is somewhat surprising since the product (**3**) is an uncoupled degenerate singlet/triplet. Thus, even though the radical is being formed, there is still significant HC bonding in **TS1**. To explore whether there is a surface crossing to the triplet state prior to forming **3**, we started with a structure similar to **TS1** but with a methyl−C−H−O angle close to 180°. This led to $\langle S^2 \rangle$ value of 0.700 and a large vibrational imaginary frequency corresponding to methyl-H abstraction by terminal oxygen. Optimization of the transition state led to a structure with a methyl−C−H−O angle of 155° and $\langle S^2 \rangle = 0.093$, suggesting that the effect of any possible spin crossing is insignificant to the relevant chemistry, and we thus did not investigate this further.

Propene activation on Bi_4O_7 leads to the products Bi_4O_7H (**3**) and an allyl radical, with a relative energy of $\Delta E = 4.1$

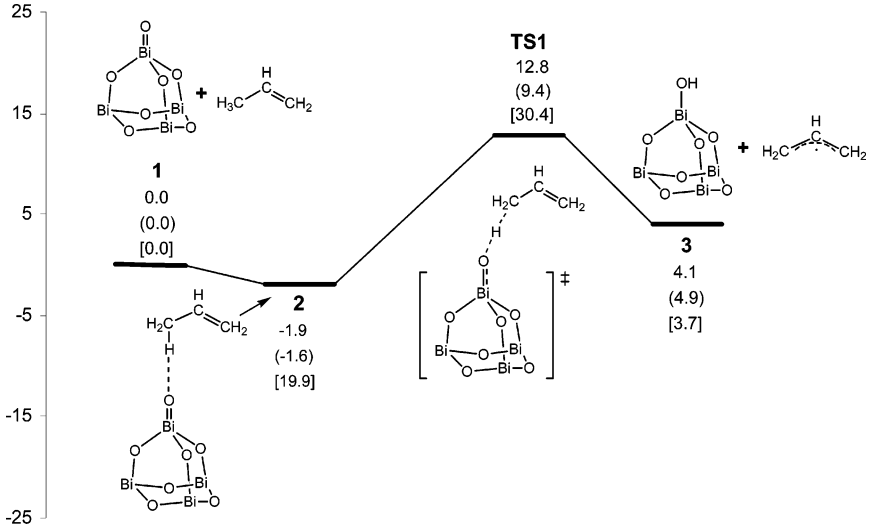

Figure 3. Singlet potential energy surface for C−H propene activation on Bi_4O_7. The Bi^V site readily activates propene, with a ΔH_{0K} barrier of 11.0 kcal/mol, just 3.0 kcal/mol lower than the $\Delta H^{\ddagger}$ observed for allyl radical formation on Bi_2O_3. The top energy is the ΔE from QM, the middle is $\Delta H_{0K} = \Delta E + \Delta ZPE$, and the bottom is ΔG_{593K}. All reported values are in kcal/mol.

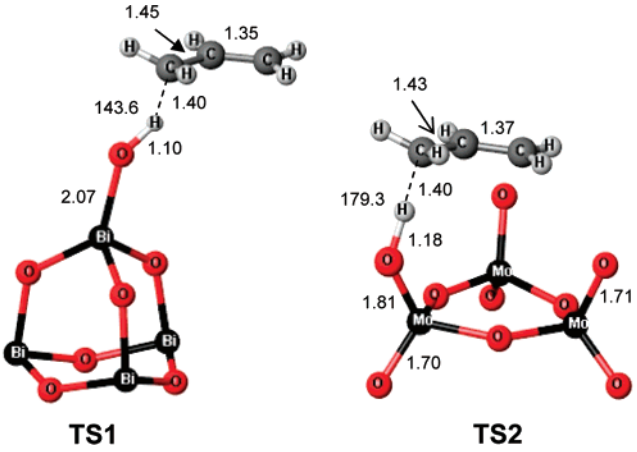

Figure 4. Structural parameters for the transition states of C−H propene activation on Bi_4O_7 (**TS1**) and Mo_3O_9 (**TS2**). Bonds lengths are shown in angstroms.

kcal/mol ($\Delta G_{593K} = 3.7$ kcal/mol). In species **3**, the Bi^V center is reduced to Bi^{IV}, with a spin density of 0.759 e^- located in a bismuth s orbital and an oxygen p orbital positioned along the Bi^{IV}−O bond. The Bi^{IV}−O bond length is 2.15 Å, while the other Bi^{III}−O bonds have an average bond length of 2.04 Å. The spin density and elongated Bi−O distance at the reduced Bi site indicate that the Bi−O bond order is about 0.5, which may assist the activation of another propene on this site to produce H_2O, Bi_4O_6, and a second allyl radical. In fact, we found that activation of propene on Bi_4O_7H (**3**) is highly exothermic ($\Delta E = -14.4$ kcal/mol, $\Delta G_{673K} = -35.9$ kcal/mol).[18] The fast consumption and restoration of Bi^V species to Bi^{III} upon reacting with another propene may explain the lack of spectroscopic evidence for the existence of Bi^V on Bi_2O_3 or bismuth molybdate catalysts.

3.1.2. Mo_3O_9 Cluster. We also investigated propene activation on Mo^{VI} (using the Mo_3O_9 cluster model) to understand the experimentally observed inability of MoO_3 to generate allyl radicals. The singlet potential energy surface for this process is shown in Figure 5. Species **5** represents the coordination of propene to molybdenum, where propene is positioned over and parallel to the Mo_3O_9 ring at the distance of ∼3 Å, with no measurable interaction between the propene π electrons and molybdenum. This weakly bound interaction has a $\Delta E = -5.1$ kcal/mol ($\Delta G_{593K} = 14.8$ kcal/mol).

We also found another coordination isomer with $\Delta E = -5.9$ kcal/mol ($\Delta G_{593K} = 17.9$ kcal/mol) in which the propene acts as a π-donor to the acidic open site of the Mo cluster at a distance of ∼2.8 Å. Since this case has the propene positioned on the side of the ring, we do not expect this structure to exhibit low-energy barriers and we consider it a less realistic mimic of the actual MoO_3 surface.

We calculate that $\Delta E^{\ddagger} = 32.5$ kcal/mol for the α-methyl hydrogen abstraction by a terminal oxygen through **TS2**, which is considerably higher than the cost for the same process on Bi^V site. Furthermore, there is a significant entropic cost of associating the propene with the surface (at 593 K, the coordination of propene to Mo_3O_9 in **5** is uphill by $\Delta G_{593K} = 14.8$ kcal/mol). This leads to a net $\Delta G^{\ddagger}_{593K} = 48.1$ kcal/mol, which is prohibitively high even at 320 °C. This agrees with the experimentally observed inactivity of MoO_3 toward propene.[4]

The imaginary normal mode for transition state **TS2** corresponds to hydrogen abstraction by the terminal oxo group, with a vibrational frequency $\nu = 1699i$ cm^{-1}. In **TS2** (see Figure 4) the O−H bond is almost formed (O−H = 1.18 Å), the C−H bond is broken (C−H = 1.40 Å), and the Mo═O bond is elongated from 1.70 to 1.81 Å, corresponding to a reduction in bond order from 2 to 1.5. Here, the two C−C bonds of the allylic portion of **TS2** are nearly equal (1.43 and 1.37 Å), which can be compared to the C−C bonds in propene of 1.50 and 1.33 Å. The $\langle S^2 \rangle$ value of 0.633 indicates open shell character, with the spin density located in the allyl π^* orbital and the molybdenum d_{zx} orbital (lying in the plane of the Mo_3O_9 ring). This is nearly identical to the spin population in intermediate **6**, which represents coordination of allyl radical to Mo_3O_9H. This analysis suggests that the allyl radical is almost fully formed in **TS2**.

The product of the first hydrogen abstraction has the allyl radical positioned on top and parallel to the Mo_3O_9H ring (**6**), which is uphill by 21.6 kcal/mol ($\Delta G_{593K} = 40.8$ kcal/mol). The $\langle S^2 \rangle$ value is 0.991, indicating an uncoupled diradicaloid singlet, with the spin density located on the allyl π^* and the molybdenum d_{zx} orbitals, the same as found for the propene activation transition state **TS2**. Thus, the reason for the high

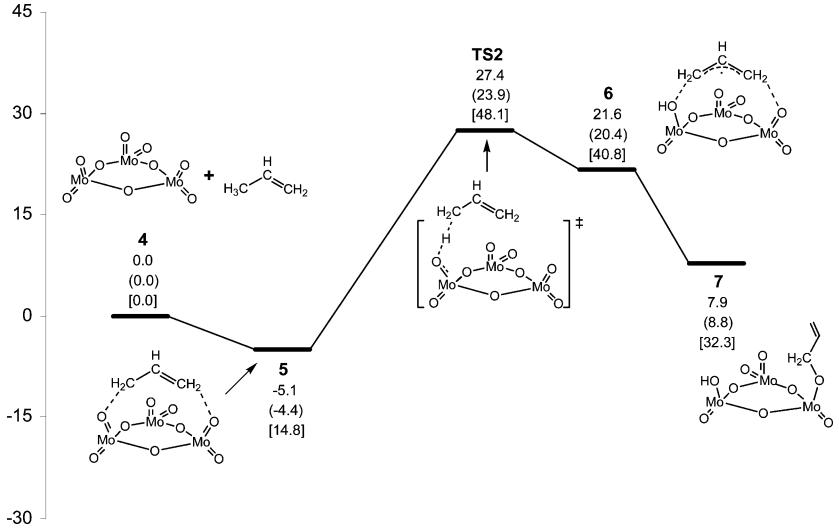

Figure 5. Singlet potential energy surface for C−H propene activation and subsequent allyl adsorption on Mo_3O_9. The high net ΔG_{593K} barrier renders MoO_3 inactive for propene oxidation. The top energy is the QM ΔE, the middle value is $\Delta H_{0K} = \Delta E + \Delta ZPE$, and the bottom one is ΔG_{593K}. All reported values are in kcal/mol.

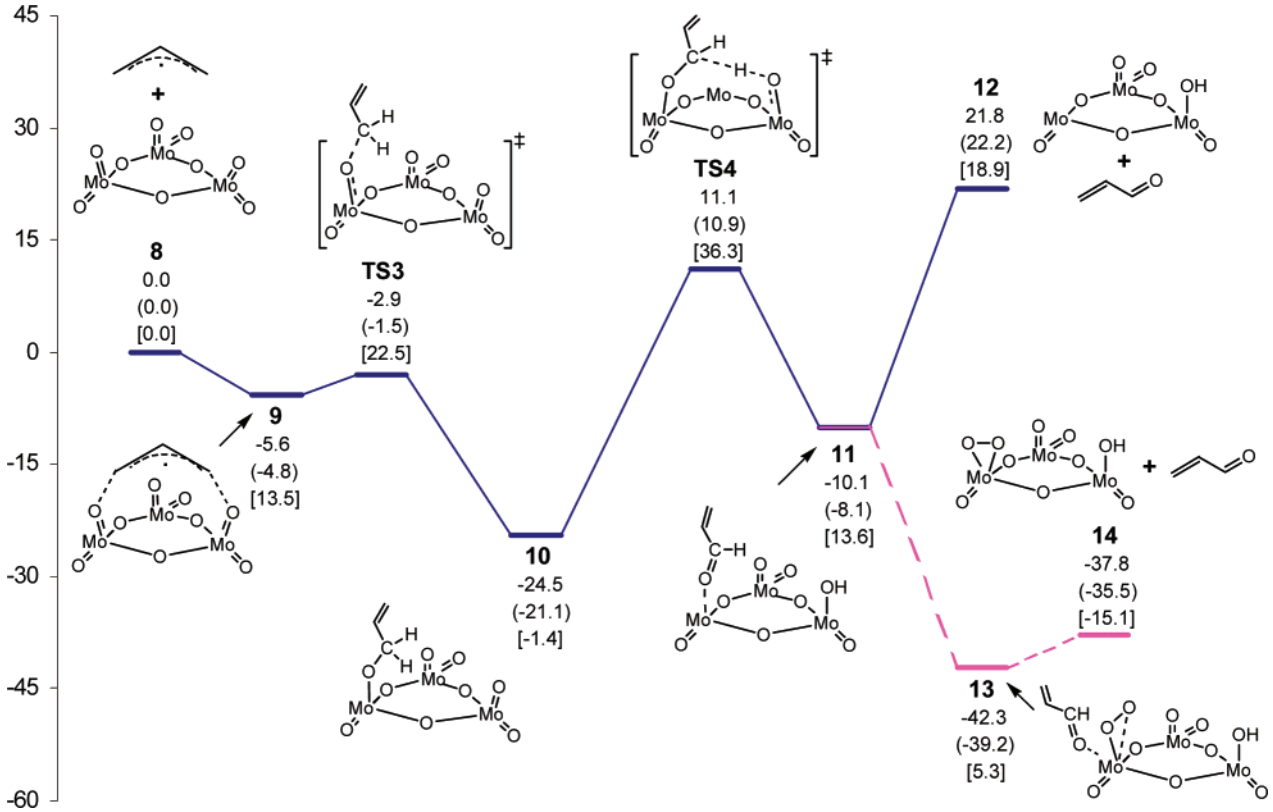

Figure 6. Potential energy surface for conversion of allyl to acrolein on Mo_3O_9 cluster (all states of spin doublets). The solid line represents the mechanism in absence of O_2, while the dashed line represents the O_2-assisted acrolein desorption. The net ΔG_{593K} barrier of 37.5 kcal/mol suggests that MoO_3 is capable of allyl oxidation, but with lower activity than bismuth molybdates. The top energy is the ΔE from QM, the middle one is $\Delta H_{0K} = \Delta E + \Delta ZPE$, and the bottom one is ΔG_{593K}. All reported values are in kcal/mol.

barrier for C−H activation on pure MoO_3 is the instability of the allyl + MoO_2OH intermediate.

Trapping of the allyl radical by a neighboring Mo═O group of Mo_3O_9H to form the open shell singlet $Mo_3O_7(OCH_2$-$CHCH_2)(OH)$ **7**, with $\langle S^2 \rangle = 0.725$, is exothermic by 13.7 kcal/mol ($\Delta G_{593K} = -8.5$ kcal/mol) with respect to **6**. Although this does not improve the kinetics of the CH activation, it is consistent with the experimental observation that MoO_3 is an effective radical scavenger.[8] The triplet state for this species is 2.2 kcal/mol higher than its respective open shell singlet, suggesting that there is some electronic coupling between the spins in **7**, albeit only a few kilocalories per mole.

3.2. Allyl Oxidation. The allyl radical formed on the bismuth oxide is expected to transfer to the molybdenum oxide before further conversion to acrolein. To study this process, we used the Mo_3O_9 cluster model with a pregenerated allyl radical. The potential energy surface for this process is shown in Figure 6, while the structural parameters for important intermediates and transition states are shown in Figure 7. Overall, the conversion of one allyl radical to acrolein is endothermic, with $\Delta E = 21.8$

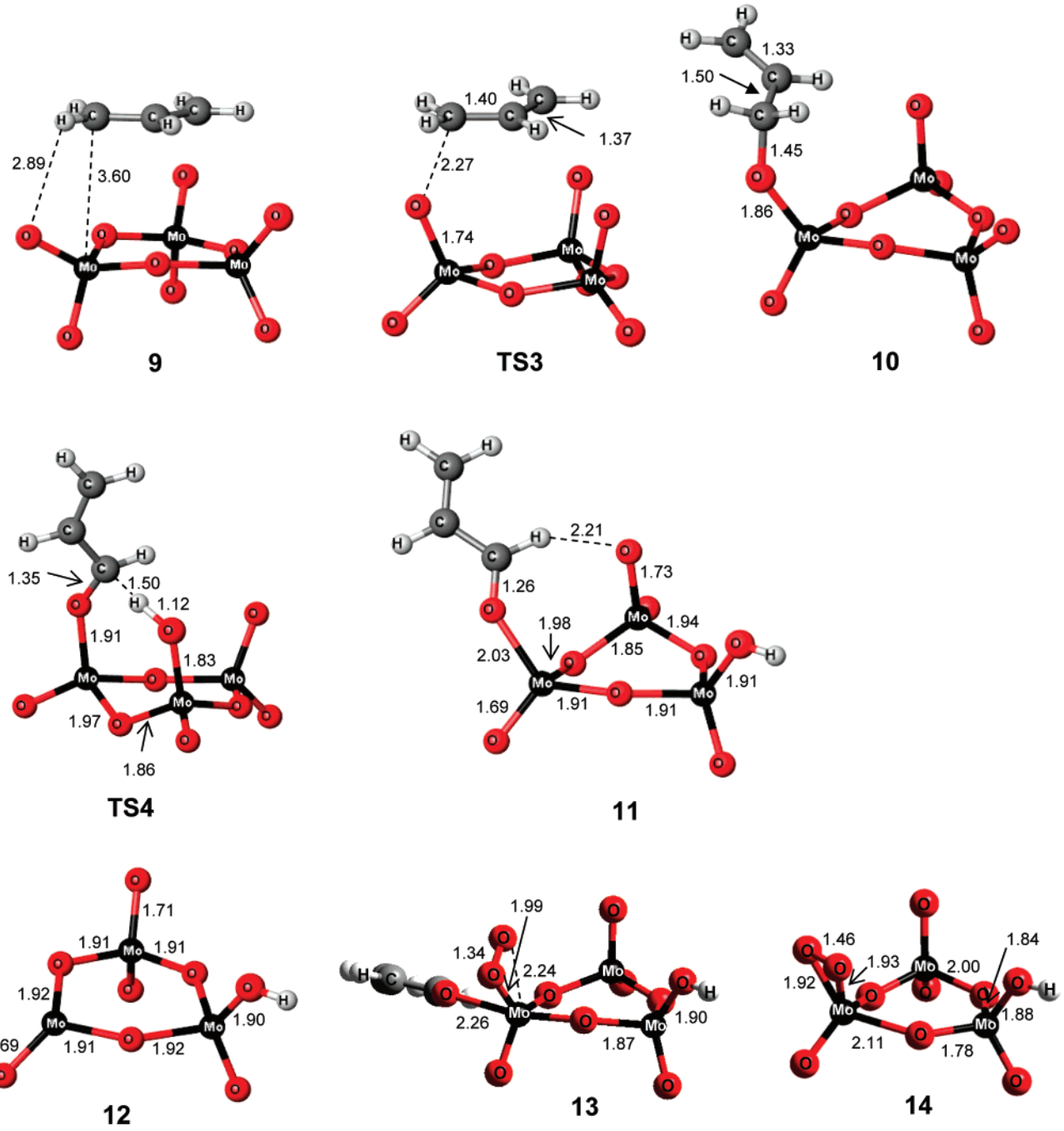

Figure 7. Structural parameters for the intermediates and transition states of the allyl oxidation on Mo_3O_9. Bond distances are shown in angstroms.

kcal/mol ($\Delta G_{593K} = 18.9$ kcal/mol). However, by including the energy of O_2 reoxidation, the overall reaction energy becomes $\Delta E = -37.8$ kcal/mol ($\Delta G_{593K} = -15.1$ kcal/mol), suggesting that the reoxidation is important for driving the overall reactivity.

3.2.1. Allyl Physisorption: π-Allyl. The first step is the coordination of the allyl radical to Mo_3O_9 (**8**) to form the π-allyl intermediate **9**, with $\Delta E = -5.6$ kcal/mol ($\Delta G_{593K} = 13.5$ kcal/mol). Intermediate **9** has the allyl positioned directly over and parallel to the Mo_3O_9 ring, with the allylic hydrogens at approximately 2.80 Å from terminal oxygens.

Another coordination isomer was found with a $\Delta E = -5.9$ kcal/mol ($\Delta G_{593K} = 16.8$ kcal/mol) in which the allyl is positioned at the side of the ring and interacting directly with the acidic site (empty coordination site) of one molybdenum atom at 2.85 Å. However, we do not expect this to lead to more favorable transition states and did not pursue this coordination further. Again, the reactivity of Mo_3O_9 toward allyl is consistent with the observed role of molybdenum oxide as an effective allyl radical scavenger.

3.2.2. Allyl Chemisorption: σ-Allyl. The π-allyl intermediate can convert to the σ-allyl intermediate **10** through a C−O bonding transition state, **TS3**, with a barrier of $\Delta E^{\ddagger} = 2.7$ kcal/mol ($\Delta G^{\ddagger}_{593K} = 9.0$ kcal/mol with respect to **9**, 22.5 kcal/mol with respect to **8**). In **TS3**, the Mo−O distance at the allyl adsorption site is 1.74 Å, whereas the C−O distance is 2.27 Å, indicating an early transition state. The transition state eigenvector has the character of C−O bond formation (with an imaginary frequency of $\nu = 169.4$i cm^{-1}). Since the ΔG_{593K} barrier for formation of σ-allyl species starting from **9** is only 9.0 kcal/mol, this process should be very rapid, as observed experimentally.[14]

The σ-allyl product, **10**, has a $\Delta E = -18.9$ kcal/mol ($\Delta G_{593K} = -14.9$ kcal/mol) with respect to **9**. The C−O bond distance in **10** is 1.46 Å (compare to 1.41 for a normal CO bond as in methanol), and the activated Mo^{V}−O bond distance is 1.86 Å (a bond order of ∼1.5). The $\langle S^2 \rangle = 0.756$, consistent with a doublet, with the spin density located in the molybdenum d_{zx} orbital, lying in the plane of Mo_3O_9 ring. A second σ-allyl conformer, with $\Delta E = -20.9$ kcal/mol ($\Delta G_{593K} = -11.1$ kcal/mol) with respect to **9**, was located as well. In this structure, the allyl is positioned exactly on the top of the Mo_3O_9 ring, which prevents it from participating in allyl conversion unless it rotates to yield the first conformer, **10**. Although this conformer is the ground state for **10**, we do not expect this to have any chemical significance.

The reverse process (i.e., the back-conversion of the σ-allyl to the π-allyl species) has a barrier of 21.6 kcal/mol ($\Delta G^{\ddagger}_{593K} = 23.9$ kcal/mol). Thus **9** → **10** should be reversible under reaction conditions. This is in the agreement with experiments, which show a rapid equilibrium between the π-allyl and the σ-allyl species.[14] However, we find **9** and **10** do not have equal energies (as postulated by Grasselli and Burrington).[17] The formation of the σ-allyl is more favorable than the π-allyl due to the energy gained from C−O bond formation, as compared to the weak interaction in π-allylic intermediate.

3.2.3. Hydrogen Abstraction. The next step in the allyl oxidation is a second hydrogen abstraction from **10** to yield **11** with a Mo^{V}−OH site and acrolein coordinated to a reduced Mo^{IV}. This occurs through a seven-membered transition state structure, **TS4**, with a calculated barrier of $\Delta E^{\ddagger} = 35.6$ kcal/mol ($\Delta G^{\ddagger}_{593K} = 37.7$ kcal/mol). The transition state eigenvector represents the hydrogen abstraction by a neighboring terminal Mo═O group (with an imaginary frequency of $\nu = 1070i$ cm^{-1}). The O−H distance in the forming bond is 1.08 Å, while the α-C−H distance has increased from 1.09 Å in **10** to 1.64 Å, and the C−O bond distance decreased from 1.46 to 1.35 Å. These bond distances indicate that the hydrogen abstraction is almost complete in **TS4**. Furthermore, the Mo═O bond at the acrolein formation site elongates from 1.86 to 1.92 Å while the Mo═O bond at the hydrogen accepting site elongates from 1.71 to 1.83 Å, consistent with the transformation of a Mo−O σ-bond to a Mo ← O coordination and of a Mo═O π-bond to a Mo−O σ-bond. The distance between the two reduced Mo atoms decreases from 3.60 to 3.36 Å, indicating a strong interaction between the two metal centers and possibly spin coupling. The $\langle S^2 \rangle$ value is 0.764, with the unpaired spin localized on the d_{yx} orbital of the Mo^{IV} atom.

Since the product, **11**, has one Mo^{V} center (spin doublet) and one Mo^{IV} center (spin triplet), we expect the ground state to be a quartet. Indeed, a second transition state (**TS4′**) was found that has a slightly lower energy ($\Delta E^{\ddagger} = 33.5$ kcal/mol, $\Delta G^{\ddagger}_{593K} = 34.0$ kcal/mol), with a significant amount of spin contamination ($\langle S^2 \rangle = 0.989$). The structure of this transition state is very similar to that of the **TS4** doublet, except that the O−H bond distance is 1.15 Å, the α-C−H distance is 1.46 Å, and the C−O distance is 1.38 Å, indicating that the O−H is not as close to being formed as in the **TS4** doublet. The spin density is located on the d_{yx} orbitals of the *two* reduced molybdenum atoms, as well as on the π^* orbital of acrolein moiety. This spin contamination suggests a low-energy quartet state, and we sought to isolate the pure quartet analogue of **TS4**, without success. Scanning of quartet potential energy surface along the forming O−H and breaking Mo═O bonds resulted in monotonic decreases in energy, where several selected points along this path have only small imaginary frequencies (less than 80i cm^{-1}) corresponding to the second hydrogen abstraction. In addition, optimization of **TS4** on the quartet surface with constrained C−H and O−H distances yielded a geometry with an imaginary frequency of 18i cm^{-1}. Consequently, it is not clear whether the lower energy of the contaminated **TS4′** is due to artificial stabilization or whether it is a true low-energy transition state. Fortunately, the difference between **TS4** and **TS4′** of −2.1 kcal/mol ($\Delta\Delta G_{593K} = -3.9$ kcal/mol) does not significantly influence our mechanistic analysis.

The experimental k_H/k_D ratio is ≈2.5 at 320 °C for the second hydrogen abstraction (obtained from molecular probe experiments using alcohol-1,1-d_2 and -3,3-d_2).[14] Our calculations lead to $k_H/k_D = 2.54$ (no tunneling corrections) using the doublet **TS4** structure, which agrees with experiment. However, our calculated KIE for **TS4′** is also 2.54, which prevents us from distinguishing the correct transition state based on KIEs. However, we expect that the transition to the spin quartet state would have little effect on the chemistry, and henceforth we will use **TS4** in our discussions on this chemistry.

Comparing the net ΔG_{593K} barriers for the second hydrogen abstraction (37.7 kcal/mol) and propene activation on Mo_3O_9 (48.1 kcal/mol), we conclude that the first process is plausible at the temperature of 320 °C, whereas the second is not. Consequently, MoO_3 should be capable of oxidizing allyl into acrolein, but it is not capable of activating propene. Furthermore, the barrier of 37.7 kcal/mol is quite high, which is in good agreement with experiments showing that allyl oxidation over MoO_3 at 320 °C yields between trace and 51.5% of acrolein, depending on the experimental setup.[4,8] This suggests that the conversion of allyl to acrolein is not particularly efficient over pure MoO_3.

TS4 (as well as **TS4′**) leads to intermediate **11**, which resembles acrolein coordinated to the reduced Mo^{IV} site. The C═O bond distance in **11** is 1.26 Å, which compares to 1.22 Å in isolated acrolein. Furthermore, the Mo ← O distance is 2.03 Å, suggesting that this acrolein precursor is still strongly coordinated to Mo site. In addition, the remaining Mo═O bond at the acrolein formation site is 0.02 Å shorter than the Mo═O in the nonreduced cluster Mo_3O_9, consistent with a stabilization effect of a spectator oxo group through the formation of a partial triple Mo−O bond, as discovered by Allison and Goddard[22] and Rappe and Goddard[42] in earlier studies on these and related systems. The $\langle S^2 \rangle$ value is 0.878, with the majority of the spin density located in the d_{xz} orbital on the Mo^{V} atom, but with the remaining density found in the d_{xy} and $d_{x^2-y^2}$ orbitals of Mo^{IV}. This is consistent with our calculations showing that the lowest spin state for the reduced Mo_3O_8 species has one Mo^{IV} and two Mo^{VI} centers, leading to the spin triplet expected for a d^2 metal with tetrahedral coordination (the open shell singlet is 5.9 kcal/mol higher in energy). Therefore, all species leading to a combination of Mo^{IV} and Mo^{V} sites are bound to suffer from spin contamination, as the quartet states become more stable. In these quartet states, two electrons are located in the d_{xy} and $d_{x^2-y^2}$ orbitals of the Mo^{IV} center, and the third electron is located in the d_{xz} orbital on the Mo^{IV} center.

3.2.4. Acrolein Desorption. The desorption of acrolein (dashed line in Figure 6) results in the reduced Mo_3O_8H species **12**, with a desorption energy $\Delta E = 31.9$ kcal/mol ($\Delta G_{593K} = 5.3$ kcal/mol), indicating a very strong binding to the reduced Mo^{IV} site. We could find no additional barrier for this desorption, and optimization of Mo_3O_8H and acrolein initially placed at a distance of 5.0 Å resulted in formation of **11** with monotonic decrease in energy. The $\langle S^2 \rangle$ value for **12** is 1.426, indicating strong spin contamination due to a quartet state that is 4.8 kcal/

mol ($\Delta\Delta G_{593K} = -5.6$ kcal/mol) lower in energy than the doublet state. The spin density of **12** is located in the d_{xz} orbital on the Mo^{V} site, and in the d_{xy} and $d_{x^2-y^2}$ orbitals on the Mo^{IV} site, where one spin is up and one spin is down. A similar spin density is present in the quartet state of **12**, except that both spins on Mo^{IV} are up, giving rise to the $m_s = {}^3/_2$ state. A lower energy isomer of **12** was found (desorption $\Delta E = 28.8$ kcal/mol, $\Delta G_{593K} = 7.7$ kcal/mol) where the OH group is bridging the two reduced molybdenum atoms; however, this structure involves the contraction of Mo−Mo distance from 3.67 to 3.12 Å. However, in a larger crystal we expect this contraction to be associated with a large energetic penalty, as this would cause a distortion of the solid-state structure. Consequently, we believe the lower energy of this intermediate to be an artifact of the model cluster used in this study and we did not use this structure for further analysis.

Species **12** has two reduced molybdenum sites, one vacant Mo^{IV} site and one $Mo^{V}-OH$ site, which probably contributes substantially to the calculated endothermicity of the process. Indeed, acrolein is expected to bind more strongly to Mo^{IV} than to Mo^{VI}, and analysis of the bridging $Mo^{IV}-O$ single bonds shows that they contract as acrolein leaves, compensating for the loss of electron density. We suspect that this process is far more effective in the MoO_3 crystal, where, in addition to bridging ether oxygens, there are *stabilized oxo* oxygens by neighboring acidic Mo sites ($r_{Mo-O} = 2.30$ Å), plus ether oxygens in the second layer directly below the molybdenum atoms of the surface layer (see the MoO_3 crystal in Figure 2). Indeed, it is possible that the surface Mo^{IV} might be reoxidized by adjacent lattice oxygens as the acrolein is desorbed, a process that strongly resembles the suggested mechanism for reoxidation of the reduced sites.[43−45]

3.2.5. Dioxygen-Assisted Acrolein Desorption. To further understand how reoxidation can affect acrolein desorption, we considered the energetics for O_2-assisted desorption of acrolein. A similar mechanism was proposed recently for oxidative dehydrogenation of propane conversion to propene over the cyclic V_4O_{10} cluster by Cheng et al.[46] This has also been applied in a recent study of CH_4 activation on Si-supported Mo═O by Chempath and Bell.[47] Although it is generally assumed that dioxygen dissociates at a site different from the catalytically active site, we considered the consequence of allowing an O_2 to coordinate with the reduced Mo^{IV} site in **11** (prior to desorption of acrolein).

We find that the coordination of O_2 promotes acrolein desorption quite significantly, destabilizing the binding of acrolein and avoiding the necessity of forming vacant, reduced Mo^{IV}.

Coordination of $^3O_2$ to **11** to form the doublet peroxy species **13** has a calculated $\Delta E = -32.2$ kcal/mol ($\Delta G_{593K} = -8.3$ kcal/mol) (red curve in Figure 6). The distance of the shorter Mo−O bond in the $Mo(O_2)$ peroxy moiety is 1.99 Å, indicating a bond order of almost 1 (0.08 Å longer than the bridging Mo−O bonds of the Mo_3O_9 cluster). The longer Mo−O bond is 2.24 Å, where the lone pair on oxygen makes donor−acceptor coordination to the Mo. The O−O bond length of 1.34 Å indicates a bond order of 1.5 (compare to 1.33 Å for HO_2 radical). The $\langle S^2 \rangle$ value of **13** is 1.187, indicating a strong spin contamination from a quartet state that is 6.8 kcal/mol higher in energy than the corresponding doublet. The spin density is located in the d_{xz} orbitals of both reduced molybdenum sites and in the OO_π orbital that contributes a bond order of 0.5 to the 1.5 bond order of the O−O moiety.

The Mo−(O═CH−CH═CH_2) distance in **13** is 2.26 Å, which is 0.23 Å longer than in **11**, indicating a significantly weakened donor−acceptor coordination. Indeed the energy to remove the acrolein is reduced from 31.9 to 4.5 kcal/mol by chemisorbing the O_2.

We also located an isomer of species **13**, where one of the peroxo oxygens also coordinates to the *second* reduced Mo atom, with a Mo−O distance of 2.38 Å (**13′**). Isomer **13′** is significantly more stable than **13** (coordination $\Delta E = -43.6$ kcal/mol, $\Delta G = -15.5$ kcal/mol), most likely due to the energy gain from partially oxidizing both reduced Mo atoms. However, to accommodate this second coordination the Mo−Mo distance reduces from 3.60 to 3.31 Å, severely distorting the cluster structure. However, much like for the isomer of **12** described above, in a larger crystal we expect this distortion to be associated with a large energetic penalty, and we did not use this structure for further analysis.

Further discussions on the nature of bonding in such metal−peroxy systems and the relation to hydrocarbon oxidations was reported in the V_4O_{10}-catalyzed oxy dehydrogenation of propane to propene by Cheng et al.[46]

Desorption of acrolein from **13** is slightly endothermic on the ΔE surface ($\Delta E = 4.5$ kcal/mol) due to the weak coordination of acrolein to acidic molybdenum, although far less endothermic than from **11** ($\Delta E = 31.9$ kcal/mol). However, on the free energy surface the desorption is now strongly exothermic ($\Delta G_{593K} = -20.4$ kcal/mol), showing that reoxidizing the reduced sites prior to desorption significantly improves this process. Dissociating acrolein from **13** produces the cyclic peroxy $Mo_3O_{10}H$ cluster **14**, which can be described as the product of a triplet O_2 with a quartet state Mo_3O_8H. Both Mo−O bond distances in the Mo−(O_2)ring are 1.93 Å, and the O−O bond distance is 1.46 Å, suggesting a single covalent O−O bond and two single covalent Mo−O bonds. The $\langle S^2 \rangle$ value is 0.758, and there is no spin contamination in this species due to the absence of a Mo^{IV} center.

As mentioned above, it is generally assumed that migration of lattice oxygens is responsible for the reoxidation of the Mo^{IV-}-(O═CH−CH═CH_2) and not molecular oxygen as in the above description. Nevertheless, these results indicate that acrolein can be desorbed easily from a surface site in the presence of available oxygens, either from the lattice or gas-phase O_2.

4. Discussion and Conclusions

4.1. First CH Activation. We calculate an activation enthalpy ($\Delta H^{\ddagger}$) for the first hydrogen abstraction on the Bi^{V} site of the Bi_4O_7 cluster to form an allyl radical of 11.0 kcal/mol ($\Delta G^{\ddagger}_{593K} = 30.4$ kcal/mol), which is close to the measured $\Delta H^{\ddagger} = 14$ kcal/mol for allyl radical formation on Bi_2O_3. We did not explore the barrier for CH activation on Bi^{III} sites, as we previously showed that the reaction Bi_4O_6 + propene → $Bi_4O_5(OH)$ + allyl is strongly endothermic ($\Delta E = 50.9$ kcal/mol ($\Delta G_{673K} = 41.6$ kcal/mol), and a barrier would thus be meaningless. However, we show here that propene activation on a Mo^{VI} site in a Mo_3O_9 cluster (representing the MoO_3 catalyst) has a barrier of 32.5 kcal/mol ($\Delta G_{593K} = 48.1$ kcal/mol), which is in good agreement with the experimental observation that MoO_3 is incapable of activating propene under conditions for which Bi_2O_3 activates propene rapidly. Most likely, this is due to the stronger Mo^{VI}═O bond as compared to the Bi^{V}═O bond, and the absence of a driving force that would lower the activation energy (such as the formation of a C═O bond).

Although we know of no direct evidence from experiment of the role of Bi^{V}, the absence of alternative mechanisms and

SCHEME 2: Mechanism and Energetics for Propene Oxidation over Bismuth Molybdate[a]

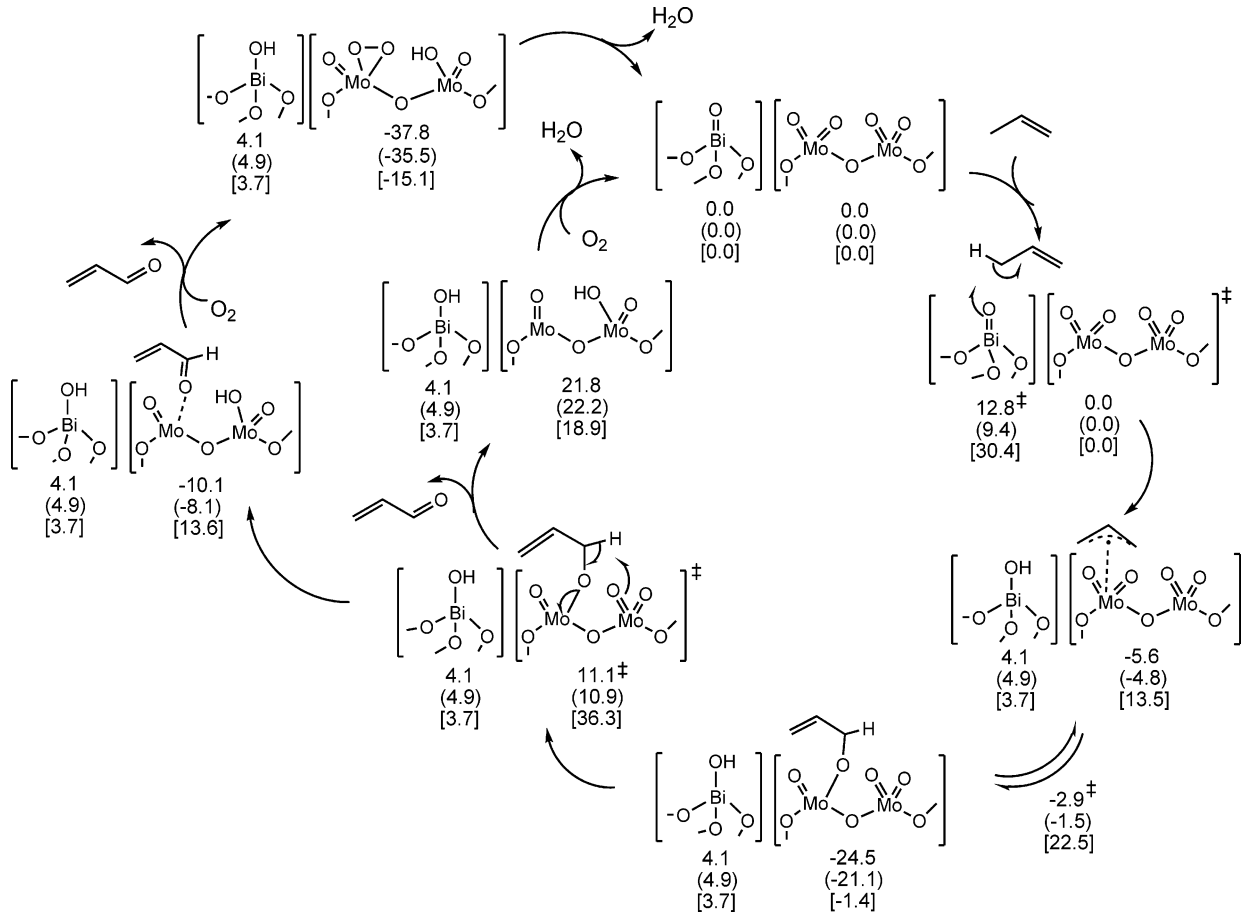

[a] The top energy is the ΔE from QM, the middle is $\Delta H_{0K} = \Delta E + \Delta ZPE$, and the bottom is ΔG_{593K}. All reported values are in kcal/mol.

the agreement in the magnitude of the activation energy with experiment further supports the conclusion from theory that Bi^V is involved. The lower value for the computed barriers as compared to the experimentally measured ones could be due to the relatively low concentration of Bi^V sites on the catalyst surface, which would seemingly increase measured activation energy. Potentially, this could also explain the significantly different activation energies reported by other experimental investigations, as a change in experimental setup could influence the number of Bi^V sites, which in turn would change the measured activation energy. This could be tested experimentally, either through testing on a surface with pregenerated Bi^V sites, or through poisoning of potential Bi^V sites on the regular Bi_2O_3 surface.

4.2. Allyl Adsorption. We find that allyl chemisorption on Bi_2O_3 is not favorable, $\Delta E = 3.8$ kcal/mol ($\Delta G_{593K} = 31.0$ kcal/mol),[18] whereas it is quite favorable on MoO_3, $\Delta E = -24.5$ kcal/mol ($\Delta G_{593K} = -1.4$ kcal/mol), which is consistent with experiment. Most likely, the reason why it is not favorable on Bi_2O_3 is the resulting reduction of Bi^{III} to the unfavorable Bi^{II} state, similar to the unfavorability of the initial CH activation step on Bi_2O_3. However, for the second step we cannot use the assumption that a Bi^V site can do the required chemistry, as the odds of the activated allyl complex finding a *second* Bi^V site should be very small, particularly compared to the probability of the allyl simply going back to propene. Thus, the chemisorption of the allyl on MoO_x is a requirement for further oxidation.

The π-allyl intermediate can rapidly convert to a σ-allyl intermediate (acrolein precursor) through the reversible formation of C−O bond, which is consistent with molecular probe experiments by Grasselli et al. (using D-labeled allyl alcohol over molybdate and bismuth molybdate catalysts).[14,17] Our calculations show that the conversion of π-allyl to σ-allyl is rapid, with a ΔG_{593K} barrier of 9.0 kcal/mol, and the reverse process (i.e., the back-conversion of the σ-allyl to the π-allyl species) has a barrier of 23.9 kcal/mol. As such, this process is reversible under oxidation conditions, which agrees with the molecular probe experiments that show a rapid π-allyl $\leftrightarrow$ σ-allyl equilibrium. We compute $k_H/k_D = 2.54$ for the second hydrogen abstraction which agrees with the experimental value of $\approx$2.5 at 320 °C. This, together with our observation that the second hydrogen abstraction is the rate-determining step for allyl conversion, explains the observed 70:30 ratio of acrolein-[3,3-d_2]:[1-d_1] produced from propene-[1,1-d_2] or propene-[3,3,3-d_3].

4.3. Second CH Activation. On Mo_3O_9, the net ΔG_{593K} barrier for abstracting the second hydrogen to form acrolein is 37.7 kcal/mol. This is the rate-determining step in the conversion of σ-allyl intermediate to acrolein, in agreement with experiment. However, the magnitude of this barrier (37.7 kcal/mol) is too high for plausible reaction rates at 320 °C, and we conclude that pure MoO_3 should not be an efficient catalyst for conversion of allyl to acrolein. This is also in good agreement with the experimental studies on allyl oxidation over pure MoO_3, which report acrolein yields of 0−51.5%, depending on the experimental conditions.

4.4. Acrolein Desorption. We found that desorption of acrolein to form a Mo^{IV} site is not favorable (endothermic by $\Delta E = 31.9$ kcal/mol, $\Delta G = 5.3$ kcal/mol), but we find that O_2

can favorably assist desorption of acrolein. Binding O_2 to the Mo^{IV}–acrolein complex is exothermic by $\Delta E = -32.2$ kcal/mol ($\Delta G = -8.3$ kcal/mol), leading to a stable Mo(acrolein)-(O_2) species from which the acrolein desorption energy is reduced to 4.5 kcal/mol ($\Delta G = -20.4$ kcal/mol).

Next, we plan to examine the full pathway for propene oxidation on a model $BiMoO_x$ mixed metal oxide cluster. Also, we are building these QM results into the ReaxFF reactive force fields[48] so that we can carry out molecular dynamics studies of these reactive processes on realistic mixed metal oxide surfaces.

5. Summary

The overall reaction mechanism, including both bismuth and molybdenum sites, is summarized in Scheme 2. We find a low-energy pathway for propene CH activation using Bi^V in Bi_4O_7 cluster model, with a calculated barrier of $\Delta E^{\ddagger} = 12.8$ kcal/mol ($\Delta G^{\ddagger} = 30.4$ kcal/mol). This process is highly endothermic on Bi^{III}, whereas the pure molybdenum oxide exhibits a significantly higher barrier, suggesting that the CH activation event occurs on (relatively rare) Bi^V sites on the Bi_2O_3 surface.

We studied the oxidation of allyl to acrolein over Mo_3O_9. This includes the adsorption of allyl to form the π-allyl and σ-allyl species, the second hydrogen abstraction, and dioxygen-assisted acrolein desorption. The absorption of allyl radical on Mo_3O_9 is exothermic on the ΔE surface, which helps offset a slight endothermicity of the allyl generation. The π-allyl complex can reversibly form a σ-allyl intermediate, with forward and reverse $\Delta E^{\ddagger}$ ($\Delta G^{\ddagger}$) barriers of 2.7 (9.0) kcal/mol and 21.6 (23.9) kcal/mol, respectively. The σ-allyl intermediate is significantly more stable than the π-allyl, with a relative energy of -24.5 kcal/mol ($\Delta G = -1.4$ kcal/mol). Acrolein is formed in a second hydrogen abstraction step from the σ-allyl intermediate and is the rate-determining step in this process with a calculated $\Delta E^{\ddagger} = 35.6$ kcal/mol ($\Delta G^{\ddagger} = 37.7$ kcal/mol). Finally, studies of acrolein desorption suggest that reoxidation of the reduced sites prior to acrolein desorption significantly improves this process.

Acknowledgment. The personnel involved in this research were partially supported by DOE (DE-PS36-03GO93015), ONR (N00014-06-1-0938), and Chevron. The facilities were supported by ARO-DURIP and ONR-DURIP funds.

Supporting Information Available: Computational details including Cartesian coordinates, energies, and vibrational frequencies. This material is available free of charge via the Internet at http://pubs.acs.org.

References and Notes

(1) Grasselli, R. K. *J. Chem. Educ.* **1986**, *63*, 216.

(2) Burrington, J. D.; Kartisek, C. T.; Grasselli, R. K. *J. Catal*. **1983**, *81*, 489.

(3) Grasselli, R. K.; Burrington, J. D.; Buttrey, D. J.; De Santo, P., Jr.; Lugmair, C. G.; Volpe, A. F., Jr.; Weingand, T. *Top. Catal.* **2003**, *23* (1−4), 5.

(4) Burrington, J. D.; Grasselli, R. K. *J. Catal*. **1979**, *59*, 79.

(5) Massoth, F. E.; Scarpiello, D. J. *J. Catal.* **1971**, *21*, 225.

(6) Swift, H. E.; Bozik, J. E.; Ondrey, J. A. *J. Catal.* **1971**, *21*, 212.

(7) Grzybowska, B.; Haber, J.; Janas, J. *J. Catal*. **1977**, *49*, 150.

(8) Martir, W.; Lunsford, J. H. *J. Am. Chem. Soc*. **1981**, *103*, 3728.

(9) Adams, C. R.; Jennings, T. J. *J. Catal.* **1963**, *2*, 63.

(10) Adams, C. R.; Jenning, T. J. *J. Catal.* **1964**, *3*, 549.

(11) Voge, H. H.; Wagner, C. D.; Stevenson, D. P. *J. Catal*. **1963**, *2*, 58.

(12) Dozono, T.; Thomas, D. W.; Wise, H. *J. Chem. Soc., Faraday Trans. 1* **1973**, *69*, 620.

(13) White, M. G.; Hightower, J. W. *AIChE J.* **1981**, *27* (4), 545.

(14) Burrington, J. D.; Kartisek, C. T.; Grasselli, R. K. *J. Catal*. **1980**, *63*, 235.

(15) Burrington, J. D.; Kartisek, C. T.; Grasselli, R. K. *J. Catal*. **1982**, *75*, 225.

(16) Burrington, J. D.; Kartisek, C. T.; Grasselli, R. K. *J. Catal*. **1984**, *87*, 363.

(17) Grasselli, R. K.; Burrington, J. D. *Ind. Eng. Chem. Prod. Res. Dev.* **1984**, *23*, 393.

(18) Jang, Y. H.; Goddard, W. A. *Top. Catal*. **2001**, *15*, 273.

(19) Jang, Y. H.; Goddard, W. A. *J. Phys. Chem. B* **2002**, *106*, 5997.

(20) DiCosimo, R.; Burrington, J. D.; Grasselli, R. K. *J. Catal*. **1986**, *102*, 234.

(21) Moro-Oka, Y.; Ueda, W. *Adv. Catal.* **1994**, *40*, 233.

(22) Allison, J. N.; Goddard, W. A. In *Active Sites on Molybdenum Surfaces, Mechanistic Considerations for Selective Oxidation and Ammoxidation of Propene*; Grasselli, R. K., Bradzil, J. F., Eds.; American Chemical Society: Washington, DC, 1985; Vol. 279, p 23.

(23) Becke, A. D. *Phys. Rev. A* **1988**, *38*, 3098.

(24) Lee, C. T.; Yang, W. T.; Parr, R. G. *Phys. Rev. B* **1988**, *37*, 785.

(25) Hay, P. J.; Wadt, W. R. *J. Chem. Phys*. **1985**, *82*, 299.

(26) *Jaguar 6.5*; Schrodinger, LLC: Portland, OR, 2005.

(27) Harwig, H. A. *Anorg. Allg. Chem.* **1987**, *444*, 151.

(28) France, M. R.; Buchanan, J. W.; Robinson, J. C.; Pullins, S. H.; Tucker, J. L.; King, R. B.; Duncan, M. A. *J. Phys. Chem. A* **1997**, *101*, 6214.

(29) Sidorov, L. N.; Minayeva, I. I.; Zasorin, E. Z.; Sorokin, I. D.; Borschevskiy, A. Y. *High Temp. Sci.* **1980**, *12*, 175.

(30) Oniyama, E.; Wahlbeck, P. G. *J. Phys. Chem. B* **1998**, *102*, 4418.

(31) Kienne, M.; Rademman, K. *Chem. Phys. Lett.* **1998**, *284*, 363.

(32) Fielicke, A.; Rademann, K. *J. Phys. Chem. A* **2000**, *104*, 6979.

(33) Bienati, M.; Bonacic-Koutecky, V.; Fantucci, P. *J. Phys. Chem. A* **2000**, *104*, 6983.

(34) Kihlborg, L. *Ark. Kemi* **1963**, *21*, 357.

(35) Van den Elzen, A. F.; Rieck, G. G. *Acta Crystallogr., Sect. B* **1973**, *29*, 2433.

(36) Berkowitz, J.; Inghram, M. G.; Chupka, W. A. *J. Chem. Phys.* **1957**, *26*, 842.

(37) Fialko, E. F.; Kikhtenko, A. V.; Goncharov, V. B.; Zamazaev, K. I. *J. Phys. Chem. A* **1997**, *101*, 8607.

(38) Fialko, E. F.; Kikhtenko, A. V.; Goncharov, V. B. *Organometallics* **1998**, *17*, 25.

(39) Fu, G.; Xu, X.; Lu, X.; Wan, H. *J. Am. Chem. Soc.* **2005**, *127*, 3989.

(40) Fu, G.; Xu, X.; Lu, X.; Wan, H. *J. Phys. Chem. B* **2005**, *109*, 6416.

(41) Matsuura, I. *J. Catal*. **1974**, *33*, 240.

(42) Rappe, A. K.; Goddard, W. A. *J. Am. Chem. Soc.* **1982**, *104*, 3287.

(43) Keulk, G. W. *J. Catal*. **1970**, *19*, 232.

(44) Krenzke, L. D.; Keulks, G. W. *J. Catal.* **1980**, *61*, 316.

(45) Glaeser, L. C.; Brazdil, J. F.; Hazel, M. A. S.; Mehecic, M.; Grasselli, R. K. *J. Chem. Soc., Faraday Trans*. **1985**, *81*, 2903.

(46) Cheng, M.; Chenoweth, K.; Oxgaard, J.; van Duin, A.; Goddard, W. A. *J. Phys. Chem. C* **2007**, *111*, 5115.

(47) Chempath, S.; Bell, A. T. *J. Catal.* **2007**, *247*, 119.

(48) Goddard, W. A., III; van Duin, A.; Chenoweth, K.; Cheng, M.; Pudar, S.; Oxgaard, J.; Merinov, B.; Jang, Y. H.; Persson, P. *Top. Catal.* **2006**, *38*, 93.